High-sensitivity detection of breast tumors *in vivo* by use of a pH-sensitive near-infrared fluorescence probe

Julia Eva Mathejczyk
Jutta Pauli
Christian Dullin
Ute Resch-Genger
Frauke Alves
Joanna Napp

High-sensitivity detection of breast tumors *in vivo* by use of a pH-sensitive near-infrared fluorescence probe

Julia Eva Mathejczyk,[a] Jutta Pauli,[b] Christian Dullin,[c] Ute Resch-Genger,[b] Frauke Alves,[a,d] and Joanna Napp[a,c]
[a]Max-Planck-Institute for Experimental Medicine, Department of Molecular Biology of Neuronal Signals, 37075 Göttingen, Germany
[b]BAM Federal Institute for Materials Research and Testing, 12489 Berlin, Germany
[c]University Medicine Göttingen, Department of Diagnostic Radiology, 37075 Göttingen, Germany
[d]University Medicine Göttingen, Department of Hematology and Oncology, 37075 Göttingen, Germany

Abstract. We investigated the potential of the pH-sensitive dye, CypHer5E, conjugated to Herceptin (pH-Her) for the sensitive detection of breast tumors in mice using noninvasive time-domain near-infrared fluorescence imaging and different methods of data analysis. First, the fluorescence properties of pH-Her were analyzed as function of pH and/or dye-to-protein ratio, and binding specificity was confirmed in cell-based assays. Subsequently, the performance of pH-Her in nude mice bearing orthotopic HER2-positive (KPL-4) and HER2-negative (MDA-MB-231) breast carcinoma xenografts was compared to that of an always-on fluorescent conjugate Alexa Fluor 647-Herceptin (Alexa-Her). Subtraction of autofluorescence and lifetime (LT)-gated image analyses were performed for background fluorescence suppression. In mice bearing HER2-positive tumors, autofluorescence subtraction together with the selective fluorescence enhancement of pH-Her solely in the tumor's acidic environment provided high contrast-to-noise ratios (CNRs). This led to an improved sensitivity of tumor detection compared to Alexa-Her. In contrast, LT-gated imaging using LTs determined in model systems did not improve tumor-detection sensitivity *in vivo* for either probe. In conclusion, pH-Her is suitable for sensitive *in vivo* monitoring of HER2-expressing breast tumors with imaging in the intensity domain and represents a promising tool for detection of weak fluorescent signals deriving from small tumors or metastases. © *2012 Society of Photo-Optical Instrumentation Engineers (SPIE).* [DOI: 10.1117/1.JBO.17.7.076028]

Keywords: optical probe; pH sensing; cyanine; *in vivo* near-infrared fluorescence imaging; fluorescence lifetime imaging; breast tumor monitoring; Herceptin.

Paper 12183 received Mar. 16, 2012; revised manuscript received Jun. 12, 2012; accepted for publication Jun. 21, 2012; published online Jul. 27, 2012; corrected Aug. 6, 2013.

1 Introduction

Near-infrared fluorescence (NIRF) imaging presents a simple, straightforward, and safe tool for the noninvasive labeling of malignant tissue in living organisms. The selective fluorometric detection of tumors requires suitable optical probes and sensitive imaging systems for signal read-out in conjunction with easy data analysis methods for clear discrimination of specific and unspecific signals.

One of the greatest problems in fluorescence imaging *in vivo* is background fluorescence originating from autofluorescence caused by endogenous molecules[1–6] that hampers the detection sensitivity of specifically bound probes. Furthermore, following intravenous (i.v.) injection, conventional always-on fluorescent probes are systematically distributed over the entire object, causing high background signals and hindering tumor detection until the targeted probe has been concentrated in the tumor and the unbound probe is cleared from the periphery. These problems can be circumvented by the use of functional tumor-specific fluorescent probes, which have increasingly been at the focus of various studies in recent years.[7–12] However, the majority of these probes are still limited in their sensitivity and specificity, regarding penetration depth and real-time imaging of biological processes *in vivo*. Therefore, there is an ever-growing demand for the development of probes with, for instance, improved tissue penetration and site- or analyte-specific signaling that display a specific fluorescence signal only when located at the tumor site and remain otherwise dark.[2,8,13,14] Of special interest here is the sensing of pH as a change in proton concentration, known to go along with numerous diseases such as inflammation or cancer.[15] The acidic phenotype of tumor cells caused by upregulation of gylcolysis emerges early in cancerogenesis and is a near-universal property for primary tumors as well as metastases.[16] pH-responsive probes are ideally nonfluorescent after their introduction into the blood circulation, thereby minimizing background fluorescence of the unbound probe. Switching on of their emission in the acidic tumor environment[16] is thus expected to yield a high tumor-specific contrast even before the unbound probe is cleared from the object.

Although the fluorometric detection of changes in pH is well established in tumor cells *in vitro* using pH-responsive dyes with emission in the visible region,[17] pH sensing *in vivo* remains challenging, as it requires NIRF dyes with pH-sensitive spectroscopic properties as a prerequisite for protonation-induced spectral and/or intensity changes that so far are rare.[2,5,13,18] Examples are norcyanine- or norsquarine-based pH probes which contain a protonable amine moiety as a part of the dye´s π-electron system such as H-ICG,[19,20] Square-650-pH,[21] and CypHer5E. Alternatively, so-called activatable

Address all correspondence to: Frauke Alves, Department of Molecular Biology of Neuronal Signals Max-Planck-Institute for Experimental Medicine, Hermann-Rein-Str. 3, 37075 Göttingen, Germany. Tel: +49 (0)551 3899 272; Fax: +49 (0) 551 3899 644; E-mail: falves@gwdg.de

probes can be used, i.e., self-quenched dye-protein conjugates with cleavable bonds.[13] Here, enzymatic cleavage of fluorophores and ligand, for example by degradation in the lysosome, results in a spatial separation of the dyes and thus in an irreversible switching on of the probe's emission.[5,10,12]

The need for higher sensitivity of *in vivo* tumor imaging encouraged us to study the potential of pH-responsive probes to improve the sensitivity of detection and monitoring of acidic tumors *in vivo*. Protonation-induced switching on of the fluorescence of pH-sensitive probes can occur at the acidic extracellular space of the tumor, but also after internalization into the acidic compartments of the targeted tumor cell. To exploit these mechanisms for the rational design of our probe, we chose a tumor-specific antibody as targeting ligand that binds to a cell membrane receptor, mediating internalization of the antibody–dye–receptor complex, leading to the transfer of the probe into the acidic endosomes and lysosomes.[9] Here, we used the antibody trastuzumab (Herceptin) as a tumor-targeting moiety for the human epithelial growth factor receptor 2 (HER2) overexpressed on the cell membrane of various tumor types,[22–24] including 25% to 30% of all breast cancers.[25] As pH-sensitive dye, we employed CypHer5E, a pentamethine dye with a protonable indole group that has a pKa *in vitro* of 7.3[26] and is perfectly suited for pH sensing in a biological environment. This fluorophore has already been shown to be functional in cell assays.[26–29] Although CypHer5E displays emission bands in the near-infrared (NIR) region and a good water solubility, contains a functional group for bioconjugation, and is a promising candidate for *in vivo* imaging of structures with a low pH (like a tumor), so far no reports have been published that describe its use for *in vivo* imaging.

In this work, the functionality and sensitivity of CypHer5E-Herceptin (pH-Her) was examined in orthotopic breast tumor mouse models with distinct HER2 expression patterns.[30,31] The results were compared to that of an Alexa Fluor 647-Herceptin (Alexa-Her) conjugate acting as representative example for an always-on probe with comparable absorption and emission spectra. For both conjugates, also compared were the advantages and limitations of lifetime (LT)-imaging versus conventional imaging in the intensity domain for *in vivo* tumor monitoring. We showed that the selective fluorescence enhancement of pH-Her solely in the acidic environment of the tumor led to an improved tumor-detection sensitivity over time compared to Alexa-Her when applying intensity imaging in combination with subtraction of background fluorescence. In contrast, LT-gated imaging did not improve the sensitivity of tumor detection *in vivo* for either probe. These pH-sensitive dye-biomolecule conjugates present one of the first examples of a new generation of more sophisticated optical probes with targeting and sensor function.

2 Materials and Methods

2.1 Fluorescent Probes

Herceptin was coupled to the NIRF dyes CypHer5E (GE Healthcare, Munich, Germany) and Alexa Fluor 647 (Invitrogen, Darmstadt, Germany) at different dye-to-protein (DP) ratios in cooperation with Squarix Biotechnology (Marly, Germany). For this purpose, different amounts of the amine-reactive *N*-hydroxysuccinimidyl (NHS) esters of these NIRF dyes (different ratios of dye NHS ester to antibody) were allowed to react with Herceptin in a buffer at basic pH, using

identical reaction conditions for both labels (e.g., solvent, pH, temperature, reaction time). The resulting dye-Herceptin conjugates were purified chromatographically using a Sephadex column and a phosphate buffer as eluent. The DP ratios were calculated from the photometrically determined concentration of the dye and the protein using a calibrated Cary 5000 spectrometer (Varian Inc., Australia) following a previously described procedure.[32] In the case of Alexa Fluor 647, the dye concentration was determined from the integral absorbance at the longest-wavelength absorption. For CypHer5E, the dye concentration was determined from the absorbance measured at 565 nm using a previously measured molar absorption coefficient of 15, 335 L/mol/cm.

2.2 Spectroscopic Analysis

2.2.1 Determination of fluorescence enhancement factor

Fluorescence emission spectra of pH-Her and Alexa-Her conjugates were measured at a concentration of 5 μg IgG in 75 μL PBS at pH 7.5 and 5.5, respectively. The pH of PBS was adjusted with 1 M NaOH and 1 M HCl solutions, using a calibrated pH meter (SevenEasy, Mettler-Toledo, Giessen, Germany). The pH values were controlled again after addition of the fluorescent probes and adjusted again to the respective value if necessary. The spectrally uncorrected fluorescence spectra[33] were obtained with a Spectrofluorometer QuantaMaster (Photon Technology International, Seefeld, Germany), immediately after pH adjustment of the probe-containing solutions, using an excitation wavelength (λ_{ex}) of 635 nm and 1-cm quartz cells. The analyses of the spectroscopic measurements were performed with the software FeliX32 Analysis 1.0.

2.2.2 Determination of fluorescence quantum yields

For the relative determination of the fluorescence quantum yields (QYs) of the conjugates at pH 5.3 using λ_{ex} of 635 nm (always performed in duplicate), absorption spectra of dilute probe and standard dye solutions were recorded on a calibrated Cary 5000 spectrometer (Varian Inc., Australia) in PBS using 1-cm quartz cells. The fluorescence spectra of these solutions were measured with a calibrated Spectronics Instruments 8100 with Glan Thompson polarizers (Spectronics Instruments)[33] in the excitation and the emission channel set to 0 and 54.7 deg, respectively. The QYs of the fluorescent probes were calculated from spectrally corrected emission spectra as previously described[34] using Oxazine 1 in ethanol as QY standard. The QY of Oxazine 1 in ethanol ($\Phi_f = 0.138$) was previously determined relative to Rhodamine 101 ($\Phi_f = 0.915$). The QY of Rhodamine 101, 0.915, was measured absolutely using a new integrating sphere setup.[34]

2.3 Cell Lines

KPL-4 (provided by J. Kurebayashi, Kawasaki Medical School, Kurashiki, Japan)[30] and MDA-MB-231 (ATCC/LGC, Wesel, Germany) breast cancer cells were propagated in standard DMEM containing 4.5 g/L glucose and l-glutamine. The medium was supplemented with 10% fetal calf serum (PAN Systems, Aidenbach, Germany). Cells were cultivated under standard cell culture conditions at 37°C in a humidified atmosphere under 5% CO_2. Tumor cells were harvested near confluence by brief trypsinization in 0.05% trypsine-EDTA solution,

washed several times, and placed in sterile PBS shortly before implantation.

2.4 Fluorescence Microscopy

Breast cancer cells were seeded on four-well chambered cover-glasses coated with poly-l-lysine at a density of 2×10^4 KPL-4 cells and 1.2×10^4 MDA-MB-231 cells per well, respectively, in 500 μL DMEM. After 48 h, the medium was removed and the cells were supplemented with 500 μL DMEM and 0.1 M HEPES buffer containing 5 μg fluorescent probes or 0.2 nmol of the free fluorophores, CypHer5E (hydrolyzed CypHer5E NHS ester) or Alexa Fluor 647 (hydrolyzed Alexa Fluor 647 NHS ester). Cells were incubated with probes for 8 h at 37°C or 4°C. Afterward, the cells were washed several times with PBS and incubated with Hoechst 33342 (2 mg/L; Invitrogen, Darmstadt, Germany) to stain the nuclei of the living cells. After 10 min, the Hoechst solution was removed and the cells were covered with 500 μL PBS and subsequently used for fluorescence microscopic studies with the Axiovert 200M (Carl Zeiss, Göttingen, Germany) equipped with a NIRF-sensitive ORCA-ER digital camera (Hamamatsu, Herrsching am Ammersee, Germany). Signals of the fluorescent probes were recorded with a 640 ± 15 nm excitation and a 690 ± 25 nm emission filter and Hoechst with a 365 ± 12.5 nm excitation and a 445 ± 25 nm emission filter, respectively. Image generation and processing were performed with the software systems AxioVision Rel.4.6. and ImageJ,[35] respectively.

2.5 Animals

All animal experiments were performed according to the animal protection law, and all animal protocols were approved by the administration of Lower Saxony, Germany. Experiments were performed on female athymic nude mice, strain NMRI-Fox1nu/nu. Two weeks before in vivo imaging, mice received chlorophyll-depleted low fluorescent food, Regime 210 (SAFE, Augy, France). Mice were maintained in a sterile environment in special cages with filter huts placed in a Scantainer (Scanbur, Koge, Denmark).

2.6 Tumor Cell Implantation

KPL-4 and MDA-MB-231 breast tumor cells were implanted in the right abdominal mammary fat pad of female nude mice at the age of 6 to 12 weeks. For this purpose, mice were anesthetized by intraperitoneal injection of 15 mg/kg xylazine and 75 mg/kg ketamine. Solutions containing the respective amount of tumor cells (5×10^6 KPL-4 cells or 1×10^6 MDA-MB-231 cells) suspended in 30 μL sterile PBS were implanted with an insulin syringe with integrated needle (30G, BD, Heidelberg, Germany) as described.[36] Afterward, mice were inspected twice a week for weight loss, general condition, and tumor formation.

2.7 In Vivo Imaging

The time domain fluorescence imager, Optix MX2 (ART, Montreal, Canada),[37] was used for intensity and LT imaging in the NIRF region. This device scans in a raster modus and measures the time between every laser excitation pulse and the detection of the first fluorescence photon using a single photon counting detector. The resulting photon time-of-flight histogram, termed temporal point spread function (TPSF), obtained for each scan point, is used to calculate the LT of

the emissive species as an exponent of the slope of the decay by underlying a single exponential model.[38] The quality of the fits was judged by the value of χ^2 for each TPSF that should be between 0.8 and 1.2 for reliable fits (OptiView software, User's Manual, Version 2.02).

The in vitro fluorescence LTs of pH-Her and Alexa-Her (3 μg IgG) and their parent fluorophores were measured in 150 μL PBS and in PBS containing 5% (mass) bovine serum albumin (BSA; PBS/BSA 5%; Sigma-Aldrich, Seelze, Germany) at pH values of 7.5 and 5.5, respectively. To determine the LT of the fluorescent probes in vivo, 10 μg pH-Her and Alexa-Her dissolved in 50 μL 0.9% NaCl were each administered subcutaneously (s.c.) in healthy nude mice.

Mice were used for in vivo fluorescence imaging experiments 1 to 4 months after tumor implantation when the tumors had reached sizes of approximately 0.3 cm^3. Mice received i.v. injections of 25 μg pH-Her or Alexa-Her or 0.8 nmol of the respective free fluorophore in 0.9% NaCl. KPL-4 tumor-bearing mice were scanned before and 1, 2, 4, 24, 48, and 72 h after probe injection, and control mice, bearing MDA-MB-231 tumors, were scanned before and 24, 48, and 72 h after probe injection. During injection and scanning, mice were anesthetized with vaporized isoflurane at concentrations of 0.8% to 1%.

Imaging was carried out using an excitation wavelength of 635 nm and a 670 ± 20 nm band pass emission filter. Scans were performed with a 1.5 mm (whole body scan) or 1.0 to 1.5 mm (excised organs) raster, and an integration time of 0.7 to 1.0 s per scan point. Data were analyzed with OptiView software 1 00 00 (ART, Montreal, Canada). Intensity values were determined in normalized counts (NC), which are independent of laser power and integration time. For the subtraction of autofluorescence, the average fluorescence intensity over the tumor region of the prescan was subtracted from all intensity maps of the respective mouse. The contrast-to-noise ratio (CNR) was calculated as the difference between the average fluorescence intensity over the tumor and over a background region divided by the standard deviation of the background signals. As a background region, the area over the lung was selected, as no specific fluorescent signals from the HER2-bound probe and no unspecific signals (from fluorescent food, for example) are to be expected.

After the in vivo experiments, the animals were sacrificed, and autopsies of mice were performed. Subsequently, the tumors were excised and the tumor sizes were measured by a caliper. Furthermore, the abdomen and the thoracic cavity were opened and lung, heart, liver, kidneys, spleen, stomach, and gut were isolated and imaged ex vivo with the Optix MX2.

3 Results

3.1 pH-Her Conjugates at Low DP Ratios Show Favorable Spectroscopic Properties

For the choice of a suitable pH-sensitive probe for in vitro and in vivo studies, dye-Herceptin conjugates of different DP ratios were spectroscopically studied with respect to their pH sensitivity and QYs. As shown in Fig. 1(a) and 1(b), a decrease in pH led to an increase in fluorescence only in the case of the pH-sensitive dye conjugate pH-Her, whereas the emission of Alexa-Her did not undergo any apparent pH-induced changes ($n = 3$). No apparent change in the spectral position of the emission maxima of either probe was observed for pH values of 5.5 and 7.5. The protonation-induced fluorescence enhancement
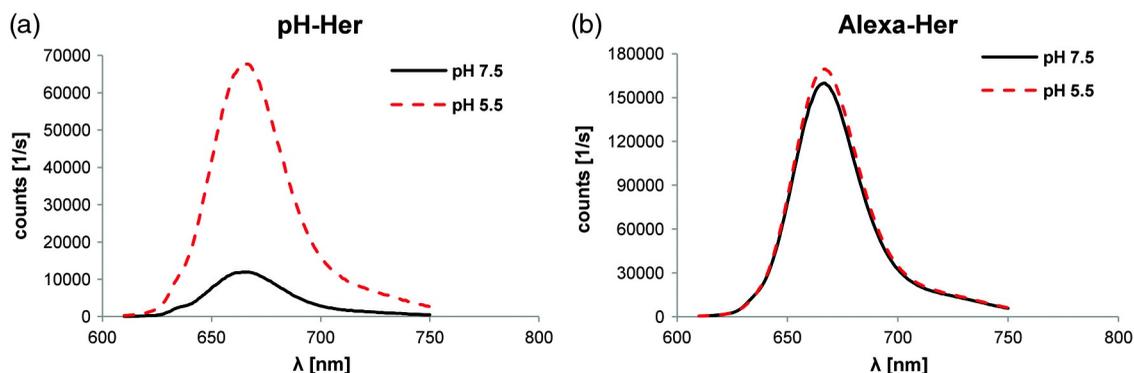
(a)

pH-Her

(b)

Alexa-Her

Fig. 1 Fluorescence emission spectra of probes at different pH. Representative uncorrected fluorescence emission spectra ($n = 3$) of pH-Her (a) and Alexa-Her (b) measured in PBS at pH of 7.5 (black curve) and of 5.5 (red dashed curve) shown as examples for conjugates with a DP ratio of 1.6 ($n = 3$); excitation was at λ_{ex} 635 nm.
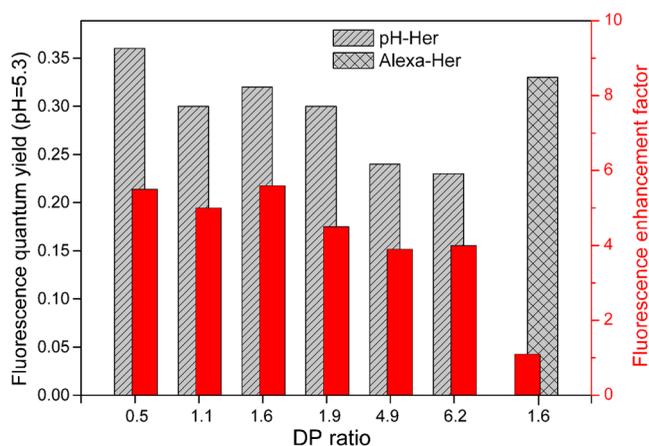

Fig. 2 Fluorescence QYs and pH sensitivities of Herceptin conjugates. Fluorescence QYs (left y-axis) of different pH-Her conjugates (gray shaded columns) and a representative Alexa-Her conjugate (gray crossed columns) in PBS at a pH of 5.3 and pH sensitivities (right y-axis) of these conjugates. The pH sensitivities are given as protonation-induced fluorescence enhancement factors (red column) calculated from the ratio of the relative fluorescence intensities at the emission maximum obtained at pH 5.5 and 7.5 ($n = 3$), respectively, as shown in Fig. 1(a) and 1(b).

factors of different dye-Herceptin conjugates and their QYs are summarized in Fig. 2. The pH sensitivity of the fluorescent conjugates was calculated as the ratio of the fluorescence intensities at the emission maximum obtained at pH values of 5.5 and 7.5 and thus presents a measure for the protonation-induced fluorescence enhancement of the probe. The maximum enhancement factor of 5.6 was found for pH-Her, with a DP ratio of 1.6, whereas pH-Her with a DP ratio of 4.9, for example, showed a 3.9-fold increase in fluorescence upon protonation. Due to its good pH sensitivity and comparably high QY, the pH-Her conjugate with a DP ratio of 1.6 [Figs. 1(a) and 2] was applied for further experiments shown in Figs. 3 to 6. The Alexa-Her conjugate with a DP ratio of 1.6 [Figs. 1(b) and 2] was used as control and as an example for an always-on probe.

3.2 Functionality of the pH-Sensitive Conjugate In Vitro

As follows from Fig. 3, the pH-sensitive probe pH-Her showed fluorescence only after receptor-mediated internalization into

HER2-positive KPL-4 cells after 8-h incubation at 37°C [Fig. 3(a), green arrow]. In contrast, after 8-h incubation at 4°C, when internalization should have been strongly reduced,[11] no signals could be detected from pH-Her that was most likely only membrane-bound [Fig. 3(b)]. These results demonstrate that pH-Her becomes emissive only after internalization, presumably when localized in the acidic endosomes and lysosomes of the target cell.[9,10,39] In contrast, the always-on probe Alexa-Her showed fluorescence after internalization [Fig. 3(c), green arrow] as well as when bound to the cell membrane [Fig. 3(c) and 3(d), orange arrow].

No fluorescence signals were detected on HER2-negative MDA-MB-231 cells after incubation with either pH-Her or Alexa-Her at 37°C and 4°C (data not shown). Incubation of both cell types for 8 h with the corresponding free fluorophores CypHer5E and Alexa Fluor 647 at 37°C and 4°C did not yield any detectable fluorescence, underlining the absence of unspecific binding and/or internalization of the dyes (data not shown).

3.3 Improved Detection Sensitivity of Tumors by the Combined Use of a pH-Sensitive Probe and Subtraction of Autofluorescence

Representative fluorescence intensity maps of KPL-4 tumor-bearing mice over time obtained after subtraction of autofluorescence are shown in Fig. 4. After i.v. application of pH-Her [Fig. 4(a), $n = 3$], the fluorescence in the tumor (white circle, shown at 24 h) can be clearly detected. The background fluorescence (white circle, shown at 24 h) is low and comparable to the fluorescence of the mouse prescan, except for some signals deriving from autofluorescence of the gastrointestinal tract.[3] In contrast, after injection of Alexa-Her [Fig. 4(b), $n = 3$], the fluorescence in the tumor (white circle, shown at 24 h) is also clearly visible, but simultaneously, the background signals resulting for this probe (white circle, shown at 24 h), are high compared to the signals from the prescan.

Hence, as rationalized with our probe design concept, use of the pH-sensitive probe pH-Her in combination with subtraction of autofluorescence enabled the elimination of major contributions of background fluorescence in scans of tumor-bearing mice. In contrast, the intensity of the background strongly increased after i.v. injection of the always-on probe Alexa-Her and could not be eliminated by subtraction of autofluorescence.

To quantify the tumor detection sensitivity *in vivo* after injection of the fluorescent probes and subtraction of autofluorescence, CNRs were calculated. As shown in Fig. 5, i.v.
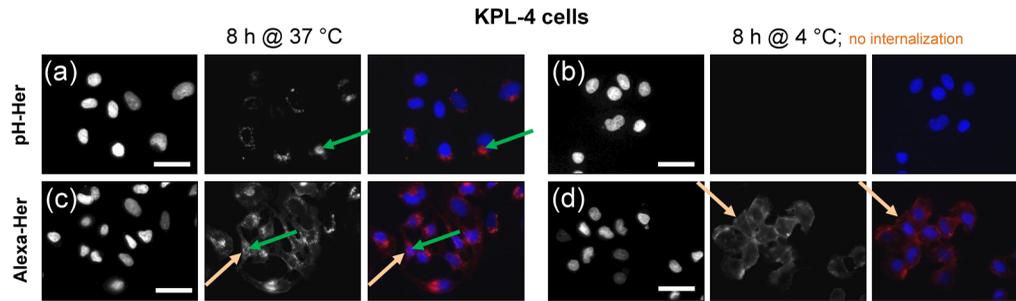
KPL-4 cells

Fig. 3 Fluorescence microscopy demonstrates internalization-dependent activation of pH-Her. Breast cancer cells grown on culture slides were incubated for 8 h with pH-Her or Alexa-Her. On the left panel, counterstain of cell nuclei with Hoechst 33342, in the middle, probe-derived signals, and on the right panel, merged images of the cell nuclei (blue) and the probe (red) are illustrated. (a), When incubated with KPL-4 cells at 37°C, pH-Her shows fluorescence only after receptor-mediated internalization (green arrow). (b), At 4°C, no signals from the pH-sensitive probe presumably bound to the cell membrane can be detected. (c), Alexa-Her shows fluorescence from the internalized probe (green arrow) and also membrane-derived fluorescence can be observed after 8 h of incubation at 37°C (c) and 4°C (d) (orange arrow, no internalization). Representative images of three independently performed experiments are presented. Bars represent 50 μm.
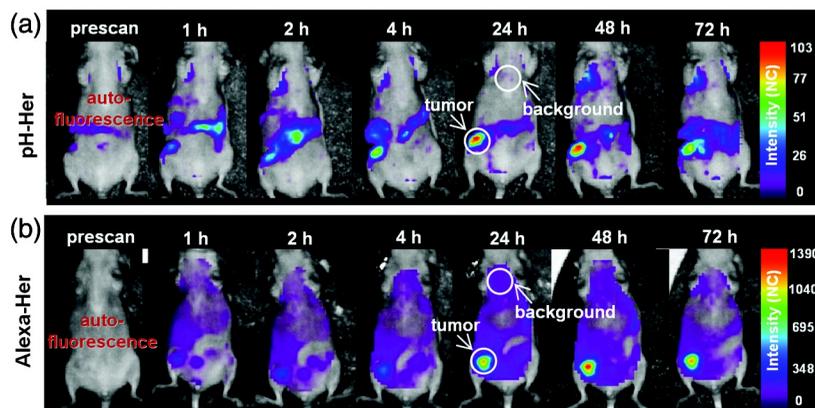

Fig. 4 *In vivo* intensity maps after probe application and subtraction of autofluorescence. KPL-4 breast tumor–bearing mice were imaged in a ventral position before (prescan) and 1 to 72 h after i.v. probe injection. Representative ($n = 3$) fluorescence intensity images after subtraction of autofluorescence are shown in NC. (a), In a mouse receiving pH-Her, probe-derived signals are mainly detected in the tumor. The enhanced autofluorescence near the forelegs is most likely caused by a higher fat content of tissue. (b), In a mouse receiving Alexa-Her, probe-derived signals are obtained in the tumor and in the background. Background and tumor areas are indicated with white circles. Note the different scale bars in (a) and (b).

injection of pH-Her [Fig. 5(a)] in KPL-4 tumor-bearing mice ($n = 5$) resulted in a continuous increase of CNRs within 24 h up to a ratio of 171 that remained comparably high for 72 h. In contrast, application of Alexa-Her [Fig. 5(b), $n = 5$] led to an increase in CNR in the mice over time of at most only 82. In consequence, although the size of the fluorescence signal resulting from Alexa-Her exceeds that of pH-Her as indicated by the different range of the scale bars in Fig. 4(a) and 4(b), the average CNR over all times in KPL-4 tumor-bearing mice treated with pH-Her was about 2.5-fold higher than for mice treated with Alexa-Her.

Control experiments performed in HER2-negative MDA-MB-231 tumor-bearing mice injected with pH-Her [Fig. 5(a), $n = 3$] revealed CNRs that are in average nine times lower than in HER2-positive KPL-4 tumor-bearing mice treated with the same probe. In the case of Alexa-Her [Fig. 5(b), $n = 3$], the average CNR after probe application was only four times higher as found in MDA-MB-231 tumor-bearing mice. This illustrates that the detection specificity of the signals deriving from HER2-positive tumors, in comparison to HER2-negative tumors, can be enhanced by use of the pH-sensitive probe.

Further control experiments in KPL-4 tumor-bearing mice with the free dyes CypHer5E [Fig. 5(a), $n = 3$] and Alexa Fluor 647 [Fig. 5(b), $n = 3$] revealed that after i.v. dye injection, CNRs were also low after 24 to 72 h (maximum ratio of 21 and 20 for CypHer5E and Alexa Fluor 647, respectively) and comparable to CNRs in HER2-negative tumor-bearing mice treated with the Herceptin conjugates. These results indicate a low nonspecific accumulation of the fluorescent probes in the tumor. This further demonstrates that the tumor-targeting moiety Herceptin is necessary for efficient accumulation of the probe in the tumor and for the achievement of high CNRs. Surprisingly, Alexa Fluor 647 administered into KPL-4 tumor-bearing mice revealed a relatively high nonspecific accumulation in the tumor with comparably high CNRs at early times after injection [Fig. 5(b), CNR of 72 after 1 h].

To analyze in more detail whether the fluorescent probes accumulate nonspecifically in other organs, KPL-4 and MDA-MB-231 tumor-bearing mice were sacrificed 72 h after injection of pH-Her, Alexa-Her, or their free parent dyes and the organs were scanned *ex vivo*. In comparison to organs of untreated mice ($n = 4$), no increased fluorescence could be detected in
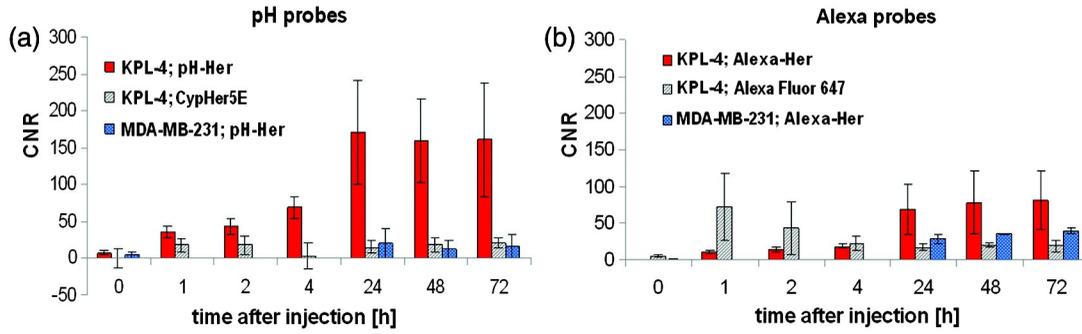
Fig. 5 Improved tumor detection sensitivity *in vivo* by use of the pH-sensitive tumor-specific probe. CNRs calculated from *in vivo* intensity scans after subtraction of autofluorescence are shown. CNRs were calculated in scans of KPL-4 tumor–bearing mice before (0 h) and 1, 2, and 4 h ($n = 3$) and 24, 28, and 72 h ($n = 5$) after i.v. injection of pH-Her (a) or Alexa-Her (b) (red columns). As controls, CNRs were also calculated from scans of KPL-4 tumor–bearing mice 0 to 72 h after i.v. injection of the free parent fluorophores CypHer5E (a) ($n = 3$) and Alexa Fluor 647 (b) ($n = 3$; gray shaded columns) as well as from scans of MDA-MB-231 tumor-bearing mice 0, 24, 48, and 72 h after injection of pH-Her (a) ($n = 3$) or Alexa-Her (b) ($n = 3$; blue columns with dots). Standard deviations are indicated as bars.

the liver, kidneys, lung, heart, spleen, stomach, or gut (data not shown).

In summary, subtraction of autofluorescence *in vivo* in combination with the use of the pH-sensitive probe pH-Her clearly improved the tumor detection sensitivity in breast tumor-bearing mice compared to the always-on probe Alexa-Her.

3.4 LT-Gated Imaging in Combination with Herceptin Conjugates Does Not Improve Tumor Detection

To assess whether LT imaging in combination with pH-Her can also provide an increased tumor detection sensitivity, LT-gated image analysis was performed with scans of KPL-4 tumor-bearing mice receiving either pH-Her or Alexa-Her. For the application of LT gates as an extra method for data illustration only, principally the LT of the probe can be determined from the *in vivo* scans in the tumor and employed for gating. However, for the identification of unknown tumor sites not macroscopically visible at the time of imaging and/or for the detection of metastases, the probe's LT must have been reliably determined from LT measurements with appropriate model systems before data

analysis with LT gating can be performed with the *in vivo* scans. This very challenging approach requires identical or at least closely matching LTs (within the chosen LT gate) for the probe in the tumor and in the model system(s). This may not be necessary fulfilled, as the LT of a fluorophore can be affected by dye environment (proticity, polarity, viscosity, refractive index) in a dye-specific manner.

Preevaluation of LTs of pH-Her [Fig. 6(a)] and Alexa-Her [Fig. 6(b)] under several application-relevant conditions (*in vitro* at different pH values and in the presence of BSA as model for plasma proteins, and *in vivo* after s.c. injection in living mice) revealed only small environment-induced changes in the fluorescence LTs of both conjugates. The presence of proteins (PBS/BSA 5%) resulted in slightly increased LTs for both probes compared to LTs in PBS. Surprisingly, the LTs of both probes obtained after s.c. injection *in vivo* were shorter compared to the LTs measured in PBS and PBS/BSA 5%, although a solution of PBS/BSA 5% has been described as a good model for the prediction of the *in vivo* LTs of several NIR cyanine dyes.[40] The mean LTs of measurements in PBS/BSA 5% at pH 7.5 and 5.5 and after s.c. injection expected to reflect the probe
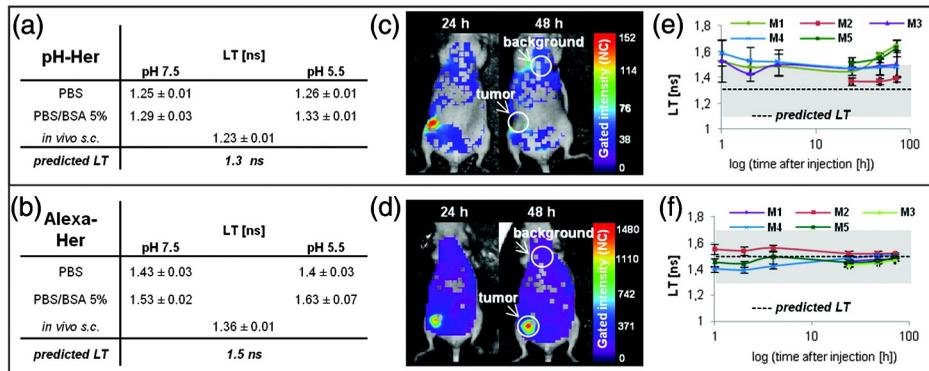

Fig. 6 LT-gating does not improve tumor detection sensitivity *in vivo*. LTs of pH-Her (a) and Alexa-Her (b) were measured in PBS and PBS/BSA 5% at pH values of 7.5 and 5.5, respectively, as well as after s.c. injection in nude mice. All measurements were performed in triplicate. The mean LT of measurements in PBS/BSA 5% and after s.c. injection for each probe was used as predicted LT for subsequent LT-gated imaging analysis in tumor-bearing mice. (c and d), Representative examples of LT-gated *in vivo* intensity maps of KPL-4 tumor-bearing mice obtained 24 and 48 h after i.v. injection of Herceptin conjugates are shown as examples. Background and tumor area are indicated with white circles at 48 h after probe injection. Fluorescence intensities with LTs of 1.3 ± 0.2 ns for a mouse receiving pH-Her (c) and with LTs of 1.5 ± 0.2 ns for a mouse receiving Alexa-Her (d) are illustrated ($n = 5$) in NC. (e and f), *In vivo* average LTs in KPL-4 tumors of mice (M1 to M5) 1, 2, and 4 h ($n = 3$) and 24, 48, and 72 h ($n = 5$) after i.v. injection of pH-Her (e) and Alexa-Her (f). The predicted LTs of the probes [determined in (a) and (b)] are indicated as black dashed lines, and the LT ranges used for LT gating of *in vivo* intensity images are shown in gray. Standard deviations are indicated as bars.

environment in the *in vivo* situation[40] were 1.3 ns for pH-Her and 1.5 ns for Alexa-Her [Fig. 6(a) and 6(b)]. These LTs (referred to as predicted LTs in the following) were used for probe identification in subsequent LT-gated *in vivo* imaging studies of tumor-bearing mice.

Subsequently, fluorescence intensity maps of KPL-4 tumor-bearing mice after i.v. injection of Herceptin-conjugates were gated with the predicted LTs of pH-Her [Fig. 6(c)] and Alexa-Her [Fig. 6(d)] as shown for scans obtained after 24 h and 48 h after probe administration ($n = 5$). Only signals with the predicted LT for the respective probe within a LT range of ± 0.2 ns are shown. Interestingly, with this approach, the fluorescence signals of pH-Her in the tumor (white circle, shown at 48 h) are partly eliminated at most times as follows from Fig. 6(c), whereas in the case of Alexa-Her, the major part of the background fluorescence is still visible [Fig. 6(d), white circle, shown at 48 h]. Similar results were obtained for scans performed at different times after probe application (data not shown). A comparison of the LT-gated images with the images obtained after subtraction of autofluorescence in the same mice (see Fig. 4) revealed that the tumor detection sensitivity could not be increased for either pH-Her or Alexa-Her with LT-gated imaging under these conditions.

Precise analyses of the average LTs in the tumor area at each scan time and in different mice showed that the LTs of pH-Her in the tumor *in vivo* with a mean value of 1.5 ns [Fig. 6(e)] are all slightly longer than the predicted LT (black dashed line). Accordingly, they are only partly covered by the LT range used for gating (1.3 ± 0.2 ns, gray area) of the pH-Her signals. This increase in LT of pH-Her in the tumor accounts for partial elimination of tumor signals. On the contrary, the average LTs of Alexa-Her in the tumor of 1.5 ns [Fig. 6(f)] agree with the predicted LT of 1.5 ns (black dashed line) and thus lie well within the chosen LT gate (1.5 ± 0.2 ns, gray area).

As to be expected, consideration of the tumor-related LT changes in the case of pH-Her and consequently, the use of a LT gate of $1.5 \text{ ns} \pm 0.2$ ns (Fig. 7) for image analysis, allowed a clear visualization of the entire tumor signals at all times as well as a partial elimination of background fluorescence.

In summary, neither for pH-Her nor for Alexa-Her could the tumor detection sensitivity *in vivo* be improved by LT-gated imaging using LTs previously determined in model systems.
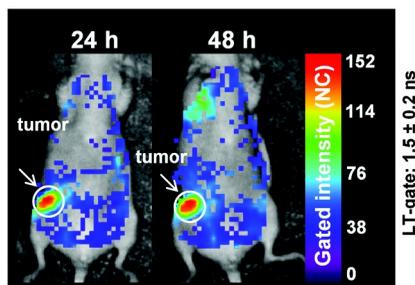

Fig. 7 LT gating of scans from KPL-4 tumor-bearing mice to the tumor-characteristic LT of pH-Her. Representative examples of LT-gated *in vivo* intensity maps of KPL-4 tumor-bearing mice obtained 24 and 48 h after injection of pH-Her are shown ($n = 5$). As an example, the same mouse as shown in Figs. 4(a) and 6(c) is depicted. In contrast to Fig. 6(c), here fluorescence intensities with LTs of 1.5 ± 0.2 ns (corresponding to the LT of pH-Her in the tumor area) are illustrated. The tumor (indicated with a white circle) is clearly visible, and parts of the background fluorescence could be eliminated.

As the predicted LT of pH-Her differed from the LT actually measured in the tumor, LT gating resulted in a considerable loss in signal. In the case of Alexa-Her, background signals deriving from unbound Alexa-Her could not be efficiently eliminated from tumor-derived fluorescence by LT gating.

4 Discussion

The present work clearly demonstrates the potential of the pH-sensitive and tumor-specific probe pH-Her to improve the tumor-detection sensitivity *in vivo* in comparison to the always-on probe Alexa-Her.

The use of pH-Her enabled the noninvasive detection of tumors *in vivo* with a 2.5-fold increase in CNR compared to the pH-insensitive control probe Alexa-Her. The very high CNRs achieved with pH-Her are due to the protonation-induced strong red shift in absorption and a considerable increase in fluorescence intensity of pH-Her in the acidic environment of the tumor and after receptor-mediated internalization in the targeted tumor cells. At the same time, pH-Her yielded only a low background fluorescence in blood, where it faces an approximately neutral pH, rendering it barely excitable at 635 nm and almost nonemissive. The remaining background fluorescence could be efficiently eliminated by subtraction of autofluorescence calculated from prescans of mice. In contrast, the always-on targeted probe Alexa-Her was fluorescent in the tumor as well as in blood, as the signal-relevant spectroscopic properties of this bioconjugate did not respond to changes in pH in the probe's environment. This resulted in high background fluorescence from unbound Alexa-Her that could not be sufficiently eliminated by subtraction of autofluorescence.

Other groups like Urano et al.[9] and Ogawa et al.[41] have also achieved high tumor-to-background ratios with pH-sensitive or pH-activatable Herceptin conjugates utilizing photon-induced electron transfer (PeT)-operated fluorescent reporters and a TAMRA-QSY7 fluorophore-quencher pair conjugated to Herceptin. However, as these probes both emit in the visible wavelength region, the limited tissue penetration hampered the generation of *in vivo* data and allowed only *ex vivo* measurements of the opened abdominal cavity of mice to detect fluorescent signals. This is of little importance for noninvasive tumor detection in living organisms desired for the sensitive visualization of pathological changes in tissue and therapy monitoring over time.

By using a NIR dye with pH-dependent absorption and emission properties, the very low background fluorescence resulting for pH-Her, which enabled high tumor-detection sensitivity, was further attained by the lack of major signals in other organs *in vivo* and *ex vivo*. In contrast to our observations, it has been reported that activatable fluorescent probes exploiting aggregation-induced fluorescence quenching, like ICG-Herceptin[10] or Cy5.5-Herceptin[12] conjugates, produce high liver signals resulting in decreased tumor contrast. Moreover, this probe design strategy that requires the conjugation of several fluorophores to one targeting ligand[12,42] cannot be used for small ligands like peptides that contain often only a single dye binding site, whereas pH-sensitive dyes[7] such as CypHer5E do not have this limitation. Moreover, the conjugation of many fluorophores to a biomolecule results in higher material costs and can reduce bioconjugate stability and binding efficiency. In addition, it can be synthetically challenging to achieve the maximum fluorescence quenching desired for probes utilizing aggregation-induced fluorescence quenching.[43]

Our probe pH-Her yielded clearly measurable signals in the tumor as early as 1 h after i.v. probe injection in KPL-4 tumor-bearing mice; the signals were considerably higher than the unspecific fluorescence arising from the gastrointestinal tract 4 h after injection. This rapid tumor detection was ascribed to an increase in fluorescence of pH-Her in the acidic tumor interstitium prior to receptor-mediated internalization in the target tumor cells. It is known that the fluorescence of CypHer5E increases immediately in the presence of protons[20,44] present in the acidic tumor environment. In contrast to pH-Her, which belongs to the few examples of targeted probes with sensor function,[13] activatable fluorescent probes exploiting distance-dependent fluorescence quenching mechanisms[10–12,41] require irreversible lysosomal degradation, which occurs only after internalization in targeted cells. In the present study, the majority of Herceptin conjugates was internalized after 8 h of incubation at 37°C in HER2-positive cells *in vitro*, confirming previous studies which illustrate the efficient internalization of fluorescent Herceptin conjugates in target cells after a similar period rather than after 1 h.[10,41] Accordingly, activatable Herceptin conjugates need a longer time for signal generation *in vivo* in the tumor. For example, Ogawa et al., who applied activatable probes for *in vivo* imaging of tumors, did not show any fluorescence images of tumor-bearing mice earlier than 24 or 48 h after i.v. injection of the probes,[10,12] suggesting that tumor contrasts at early times were low. The fast response of our probe pH-Her can be exploited for faster tumor detection.

With our pH-responsive probe pH-Her, we could achieve a very high tumor detection sensitivity with simple fluorescence intensity imaging via straightforward elimination of background fluorescence by subtraction of autofluorescence. More sophisticated LT-gated imaging requiring expensive equipment did not improve tumor detection sensitivity *in vivo*, as the LT of pH-Her in the tumor changed unpredictably compared to LTs of this probe in different model systems ranging from PBS/BSA 5% with pH values of 7.5 and 5.5 to s.c. injected healthy mice [see Figs. 6(a), 6(e), and 7]. Therefore, in pH-Her-treated KPL4 tumor-bearing mice, the majority of tumor signals revealing a LT of 1.5 ns was eliminated after LT-gating of the images using a LT gate of 1.3 ns $\pm$ 0.2 ns derived from measurements in these model systems. Obviously, some factors in the tumor environment influence the LT of pH-Her, which could not be assessed by our model systems. Further studies are required to examine the conditions in detail that could be responsible for the increase in LT of pH-Her in the tumor *in vivo*. In the case of Alexa-Her, the similar LTs in the tumor and background region did not enable an efficient discrimination of background fluorescence by LT-gated imaging. The high background signals of the Alexa-Her conjugates are attributed to the prolonged blood circulation time of IgGs.[45] In comparison, in the case of probes like RGD-Cy5.5 containing small peptides as targeting ligand that are cleared more rapidly from the blood, LT-gated imaging could be successfully applied as a tool to increase detection sensitivity of specific signals *in vivo*.[3] This indicates that in the case of always-on dye conjugates, the efficiency of LT-gated imaging is also affected by the kinetics of the tumor-targeting moiety.

In addition, our findings underline the need to better understand the origin of dye- and environment-specific changes in LT[3,46,47] to avoid signal misinterpretations. Obviously, for accurate LT gating, extensive preevaluation of the LTs of the chosen probe is necessary for each tumor model. Factors known to influence the LTs of fluorescent dyes and probes are, for example, the presence of proteins and lipids, pH, calcium concentration, and tissue depth.[3,4,40,46] Therefore, the efficiency of LT-gated imaging to eliminate background fluorescence and unspecific signals and thus, to improve tumor contrast, depends not only on the characteristics of the fluorescent probe (the chosen dye and ligand), but also on the tumor model and the imaging parameters applied. Principally, if controllable and predictable, a change in probe LT selectively at the tumor site can have great potential for the sensitive detection and monitoring of tumors and tumor spread *in vivo*, with LT-gated imaging enabling straightforward background suppression.[48]

In conclusion, this study illustrates for the first time the suitability of CypHer5E bound to Herceptin for *in vivo* tumor imaging and its potential to provide an enhanced detection sensitivity and enable faster signal detection compared to commonly applied always-on tumor-targeting probes such as the Alexa Fluor 647 Herceptin-conjugate. The selective enhancement of the emission of pH-Her is switched on only at the acidic pH of the tumor. In combination with the subtraction of autofluorescence, this provides a significantly improved detection sensitivity of breast tumors *in vivo*. This simple signaling strategy can be extended to other probes and targets. It remains to be shown whether the unexpected changes in LT observed for pH-Her in tumor tissue compared to its LT in different model systems is a characteristic of the dye, CypHer5E. In the future, the pH-responsive dye CypHer5E, conjugated to tumor-specific ligands, may be applied for the fast and sensitive detection of weak signals, deriving for instance from small metastatic lesions *in vivo*. Although the NIR fluorophore Indocyanine Green (ICG) is currently the only dye approved by the US Food and Drug Administration for use in patients,[49] pH-sensitive targeted probes such as CypHer5E conjugated to antibodies specifically binding to tumor-associated antigens like HER2 and other targeted probes with a sensor function are expected to have a bright future in medical imaging and implementation in clinical applications to detect tumor lesions *in vivo* or to monitor therapy efficiency in cancer patients over time with high sensitivity.

Acknowledgments

References

1. S. A. Hilderbrand and R. Weissleder, "Near-infrared fluorescence: application to in vivo molecular imaging," *Curr. Opin. Chem. Biol.* **14**(1), 71–79 (2010).

2. F. Alves, J. Napp, and J. E. Mathejczyk, "Optical imaging in vivo with a focus on paediatric disease: technical progress, current preclinical and clinical applications and future perspectives," *Pediatr. Radiol.* **41**(2), 161–175 (2011).

3. J. E. Mathejczyk et al., "Spectroscopically well-characterized RGD optical probe as a prerequisite for lifetime-gated tumor imaging," *Mol. Imaging* **10**(6), 469–480 (2011).

4. E. McCormack et al., "In vivo optical imaging of acute myeloid leukemia by green fluorescent protein: time-domain autofluorescence

decoupling, fluorophore quantification, and localization," *Mol. Imaging* **6**(3), 193–204 (2007).

5. H. Kobayashi and P. L. Choyke, "Target-cancer-cell-specific activatable fluorescence imaging probes: rational design and in vivo applications," *Acc. Chem. Res.* **44**(2), 83–90 (2011).

6. J. Napp et al., "Time-domain in vivo near infrared fluorescence imaging for evaluation of matriptase as a potential target for the development of novel, inhibitor-based tumor therapies," *Int. J. Cancer* **127**(8), 1958–1974 (2010).

7. H. Lee et al., "Near-infrared pH-activatable fluorescent probes for imaging primary and metastatic breast tumors," *Bioconjug. Chem.* **22**(4), 777–784 (2011).

8. R. Weissleder et al., "*In vivo* imaging of tumors with protease-activated near-infrared fluorescent probes," *Nat. Biotechnol.* **17**(4), 375–378 (1999).

9. Y. Urano et al., "Selective molecular imaging of viable cancer cells with pH-activatable fluorescence probes," *Nat. Med.* **15**(1), 104–109 (2009).

10. M. Ogawa et al., "In vivo molecular imaging of cancer with a quenching near-infrared fluorescent probe using conjugates of monoclonal antibodies and indocyanine green," *Cancer Res.* **69**(4), 1268–1272 (2009).

11. M. Ogawa et al., "H-type dimer formation of fluorophores: a mechanism for activatable, in vivo optical molecular imaging," *ACS Chem. Biol.* **4**(7), 535–546 (2009).

12. M. Ogawa et al., "In vivo target-specific activatable near-infrared optical labeling of humanized monoclonal antibodies," *Mol. Cancer Ther.* **8**(1), 232–239 (2009).

13. K. Licha and U. Resch-Genger, "Probes for optical imaging: new developments," *Drug Discov. Today* **8**(2–4), e87–e94 (2011).

14. J. Napp et al., "Targeted luminescent NIR polymer-nanoprobes for in vivo imaging of tumor hypoxia," *Anal. Chem.* **83**(23), 9039–9046 (2011).

15. P. A. Schornack and R. J. Gillies, "Contributions of cell metabolism and H+ diffusion to the acidic pH of tumors," *Neoplasia* **5**(2), 135–145 (2003).

16. R. A. Gatenby and R. J. Gillies, "Why do cancers have high aerobic glycolysis?," *Nat. Rev. Cancer* **4**(11), 891–899 (2004).

17. C. Stock et al., "pH nanoenvironment at the surface of single melanoma cells," *Cell Physiol. Biochem.* **20**(5), 679–686 (2007).

18. J. Han and K. Burgess, "Fluorescent indicators for intracellular pH," *Chem. Rev.* **110**(5), 2709–2728 (2010).

19. Z. Zhang and S. Achilefu, "Design, synthesis and evaluation of near-infrared fluorescent pH indicators in a physiologically relevant range," *Chem. Commun.* (47), 5887–5889 (2005).

20. T. Nagano, K. Kiyose, and H. Kojima, "Functional near-infrared fluorescent probes," *Chem. Asian J.* **3**(3), 506–515 (2008).

21. Y. A. Povrozin et al., "Near-infrared, dual-ratiometric fluorescent label for measurement of pH," *Anal. Biochem.* **390**(2), 136–140 (2009).

22. D. J. Slamon et al., "Studies of the HER-2/neu proto-oncogene in human breast and ovarian cancer," *Science* **244**(4905), 707–712 (1989).

23. A. Berchuck et al., "Overexpression of HER-2/neu is associated with poor survival in advanced epithelial ovarian cancer," *Cancer Res.* **50**(13), 4087–4091 (1990).

24. X. F. Le, F. Pruefer, and R. C. Bast Jr, "HER2-targeting antibodies modulate the cyclin-dependent kinase inhibitor p27Kip1 via multiple signaling pathways," *Cell Cycle* **4**(1), 87–95 (2005).

25. D. J. Slamon et al., "Human breast cancer: correlation of relapse and survival with amplification of the HER-2/neu oncogene," *Science* **235**(4785), 177–182 (1987).

26. A. Beletskii et al., "High-throughput phagocytosis assay utilizing a pH-sensitive fluorescent dye," *Biotechniques* **39**(6), 894–897 (2005).

27. E. Nordberg et al., "Cellular studies of binding, internalization and retention of a radiolabeled EGFR-binding affibody molecule," *Nucl. Med. Biol.* **34**(6), 609–618 (2007).

28. L. Gostring et al., "Quantification of internalization of EGFR-binding Affibody molecules: methodological aspects," *Int. J. Oncol.* **36**(4), 757–763 (2010).

29. Y. Hua et al., "A readily retrievable pool of synaptic vesicles," *Nat. Neurosci.* **14**(7), 833–839 (2011).

30. J. Kurebayashi et al., "Isolation and characterization of a new human breast cancer cell line, KPL-4, expressing the Erb B family receptors and interleukin-6," *Br. J. Cancer* **79**(5–6), 707–717 (1999).

31. J. M. du Manoir et al., "Strategies for delaying or treating in vivo acquired resistance to trastuzumab in human breast cancer xenografts," *Clin. Cancer Res.* **12**(3 Pt 1), 904–916 (2006).

32. M. Grabolle et al., "Determination of the labeling density of fluorophore-biomolecule conjugates with absorption spectroscopy," *Bioconjug. Chem.* **23**(2), 287–292 (2012).

33. U. Resch-Genger et al., "Traceability in fluorometry: Part Spectral II. fluorescence standards," *J. Fluoresc.* **15**(3), 315–336 (2005).

34. C. Wurth et al., "Integrating sphere setup for the traceable measurement of absolute photoluminescence quantum yields in the NIR," *Anal. Chem.* **84**(3), 1345–1352 (2012).

35. T. J. Collins, "ImageJ for microscopy," *Biotechniques* **43**(Suppl 1), 25–30 (2007).

36. J. Missbach-Guentner et al., "Morphologic changes of mammary carcinomas in mice over time as monitored by flat-panel detector volume computed tomography," *Neoplasia* **10**(7), 663–673 (2008).

37. G. Ma, P. Gallant, and L. McIntosh, "Sensitivity characterization of a time-domain fluorescence imager: eXplore Optix," *Appl. Opt.* **46**(10), 1650–1657 (2007).

38. C. Dullin et al., "Semiautomatic landmark-based two-dimensional-three-dimensional image fusion in living mice: correlation of near-infrared fluorescence imaging of Cy5.5-labeled antibodies with flat-panel volume computed tomography," *Mol. Imaging* **8**(1), 2–14 (2009).

39. D. Harari and Y. Yarden, "Molecular mechanisms underlying ErbB2/HER2 action in breast cancer," *Oncogene* **19**(53), 6102–6114 (2000).

40. W. J. Akers et al., "Predicting in vivo fluorescence lifetime behavior of near-infrared fluorescent contrast agents using in vitro measurements," *J. Biomed. Opt.* **13**(5), 054042 (2008).

41. M. Ogawa et al., "Fluorophore-quencher based activatable targeted optical probes for detecting in vivo cancer metastases," *Mol. Pharm.* **6**(2), 386–395 (2009).

42. Y. Hama et al., "A self-quenched galactosamine-serum albumin-rhodamineX conjugate: a 'smart' fluorescent molecular imaging probe synthesized with clinically applicable material for detecting peritoneal ovarian cancer metastases," *Clin. Cancer Res.* **13**(21), 6335–6343 (2007).

43. A. J. Villaraza, D. E. Milenic, and M. W. Brechbiel, "Improved speciation characteristics of PEGylated indocyanine green-labeled Panitumumab: revisiting the solution and spectroscopic properties of a near-infrared emitting anti-HER1 antibody for optical imaging of cancer," *Bioconjug. Chem.* **21**(12), 2305–2312 (2010).

44. M. E. Cooper et al., "pH-sensitive cyanine dyes for biological applications," *J. Fluoresc.* **12**(3–4), 425–429 (2002).

45. Y. Matsumura and H. Maeda, "A new concept for macromolecular therapeutics in cancer-chemotherapy: mechanism of tumoritropic accumulation of proteins and the antitumor agent SMANCS," *Cancer Res.* **46**(12), 6387–6392 (1986).

46. R. M. Andersson et al., "Characterization of probe binding and comparison of its influence on fluorescence lifetime of two pH-sensitive benzo [c]xanthene dyes using intensity-modulated multiple-wavelength scanning technique," *Anal. Biochem.* **283**(1), 104–110 (2000).

47. R. M. Andersson et al., "Fluorescence lifetime imaging of pH in cells: investigation of factors influencing the pH calibration lifetime," *Opt. Diag. Living Cells* **1**(15), 242–248 (2000).

48. M. Solomon et al., "Detection of enzyme activity in orthotopic murine breast cancer by fluorescence lifetime imaging using a fluorescence resonance energy transfer-based molecular probe," *J. Biomed. Opt.* **16**(6), 066019 (2011).

49. K. Kubota et al., "Intraoperative assessment of reconstructed vessels in living-donor liver transplantation, using a novel fluorescence imaging technique," *J. Hepatobiliary Pancreat. Surg.* **13**(2), 100–104 (2006).